

Rotating Cylinder Electrode for Velocity Sensitivity Testing*

D. C. SILVERMAN*

Abstract

Fluid flow can affect the rate of corrosion. The problem has been to determine when this effect occurs in equipment, especially before the equipment is designed. A new velocity sensitivity test using a rotating cylinder electrode is being used for this purpose. The strength of the apparatus is its defined hydrodynamics. The test procedure rests on the assumption that by operating the rotating cylinder electrode in the range of the wall shear stresses expected in the plant geometry, the mechanism by which fluid flow affects corrosion rate may be simulated in the laboratory. Once the mechanism is defined, the appropriate relationship (if known) between fluid flow rate and corrosion rate for the plant geometry can be used to predict the expected corrosion rate in the plant. This approach is demonstrated with a practical example.

Introduction

Fluid flowing past a corroding surface often affects the way an alloy corrodes in an environment. Numerous studies have discussed this phenomenon. Processes examined have included corrosion of mild steel in concentrated sulfuric acid,¹ corrosion of mild steel in oxygenated water,² and corrosion of copper-nickel alloys in seawater.³ An acceleration of the corrosion rate caused by fluid moving past the alloy surface would make corrosion rate predictions based on stagnant tests inaccurate. Indeed, this inaccuracy was recognized long ago, and test methods have been developed which attempt to define qualitatively the effect of fluid velocity. These methods include the use of laboratory flow loops⁴ and the paddle and support ring arrangement, or so-called "Landrum Wheel."⁵

Both of these techniques suffer from drawbacks. Even though the pipe loop should be able to simulate pipe flow in the plant in a quantitative fashion, the equipment associated with it makes this apparatus cumbersome for routine laboratory use. Large amounts of fluid are required, a shortcoming when the need is to examine the effects of highly corrosive or toxic fluids. In addition, the use of the pipe loop still leaves a need for a method of interfacing the pipe loop results with other geometries such as pumps, reactors, and tanks.

The Landrum Wheel, though much less cumbersome to use, operates under conditions of undefined hydrodynamics. The results are semiquantitative at best and are often qualitative. Though the results can show trends, they rarely can be used to predict actual corrosion rates in plant service. No mechanistic insight is provided by this tool. Therefore, the need still exists for a tool to determine how fluid velocity can affect corrosion. This tool must combine the well-defined hydrodynamics found in the pipe loop and the ease of assembly and disassembly of the Landrum Wheel. Only in this way will the tool be useable on a routine basis and be able to give quantitative and mechanistic insight into the corrosion rate expected in the plant.

One type of geometry that has been used to examine the effects of fluid velocity on corrosion mechanisms and rates is

the rotating electrode. Three types have been used: the rotating disk,⁶ the rotating hemisphere,⁷ and the rotating cylinder within a cylinder.⁸ Indeed, attempts have been made to relate mass transfer controlled corrosion rates found with rotating disks⁹ and cylinders¹⁰ to the corrosion rates expected in pipes. The procedure used by these authors has been to assume that the effect of flow in the laboratory geometry models the effect of flow in pipes when the rates of mass transfer in the two geometries are equal. The corresponding hydrodynamic relations that express the mass transfer rate in terms of Reynolds and Schmidt numbers are equated. This relation is solved so that the pipe velocity is expressed in terms of the corresponding rotation rate.

This method of quantitatively relating the different geometries has several weaknesses. The rotating disk operates under laminar flow conditions for a wide range of rotation rates.⁶ The above procedure of equating mass transfer rates could lead to using a disk operating under laminar flow conditions to model a pipe operating under turbulent flow conditions. Such a procedure has no theoretical justification since the fluid physics are different. This procedure is flawed when applied to the rotating cylinder even though it tends to operate under turbulent flow conditions to very low rotation rates,⁸ and turbulent flow is encountered in most plant operations involving pipe flow. The equating of mass transfer rates in this case is based on the premise that if both geometries operate in the turbulent regime, then a direct quantitative relation always exists between mass transfer rates, the Sherwood numbers, or the corresponding product of Reynolds and Schmidt numbers. Since velocity profiles and the friction factor dependencies on Reynolds numbers are different in both geometries, the hypothesis of directly equating the mass transfer relations in the two geometries is weak. In fact, this procedure has no validity if the fluid velocity effect is caused by erosion rather than convective mass transfer. Under these conditions, knowledge of the Sherwood number has no relevance with respect to corrosion rates.

Therefore, a different approach has been followed to develop a method of using the results from a rotating cylinder electrode to determine if and how fluid flow might be affecting the corrosion rate in the plant. The goal of the method is to

*Submitted for publication May 1983; revised July 1983.

*Monsanto Company, St. Louis, Missouri.

predict the effect of hydrodynamics on corrosion under all types of fluid velocity conditions. These conditions would include complete mass transfer control, partial mass transfer control, erosion, etc. This paper describes the theory behind the proposed approach to model corrosion mechanisms and the results from an actual application.

Theory of Laboratory Simulation

The use of one geometry to determine how fluid flow affects corrosion rate in another geometry is based on one important assumption: If a corrosion rate is sensitive to fluid velocity in one geometry, conditions can be constructed so that the same mechanism behind this sensitivity is present in the simulating geometry. The problem is that one often does not know if the corrosion rate in the plant geometry is sensitive to fluid velocity. The goal then is to construct the laboratory experiment so that by fulfilling certain conditions if a sensitivity is found in the laboratory, the same type of sensitivity governed by the same mechanism would be expected under the plant conditions. Then the appropriate relationship between hydrodynamics and corrosion rate for the plant geometry and for that mechanism would be used to determine the actual quantitative effect that fluid velocity has on the corrosion rate. Therefore, the major obstacle to designing such a laboratory test is the defining of the condition(s) that must be fulfilled for the test to simulate the mechanism in the plant geometry.

Two quantities that influence the effect of fluid velocity on corrosion are the hydrodynamic boundary layer and the rate of momentum transfer from the fluid bulk to the wall. Three physical quantities that contain information on the interplay between the alloy surface and the hydrodynamic boundary layer are the friction factor, the Reynolds number, and the fluid velocity. The friction factor gives a measure of the condition (roughness) of the alloy surface and how this surface affects momentum transfer and the hydrodynamic boundary layer. The Reynolds number, the ratio of convective forces to viscous forces in the fluid,¹¹ defines the flow regime—laminar or turbulent.

The fluid velocity is needed to estimate the rate of momentum transfer from the fluid to the surface; it gives an idea of the magnitude of the velocity change between the free stream and the surface. These quantities can be used to define the hydrodynamics. Once the hydrodynamics are known, such quantities as the Nusselt number (heat transfer coefficient) and the Sherwood number (mass transfer coefficient) often can be estimated by using an equation such as that determined by the Chilton-Colburn analogy.¹² All that is needed is an estimate of the ratio of the hydrodynamic and heat transfer, or hydrodynamic and mass transfer boundary layers. These ratios are available through the Prandtl and Schmidt numbers.

To construct the test one must hypothesize that if appropriate measures of the interaction between the alloy surface and the transfer of momentum are equivalent in the two geometries, then the laboratory simulation has a reasonable chance of duplicating the velocity sensitive mechanism found in the plant geometry for the same alloy and environment. The shear stress is one such measure of the alloy surface-fluid interaction. The fluid shear stress at the wall is defined by Equation (1),¹¹ assuming no slip at the wall:⁽¹⁾

$$\tau = \frac{f}{2} \rho u^2 \quad (1)$$

The shear stress at the wall, τ , measures the rate of momentum transfer to the wall. The friction factor is the resistance to fluid flow created by the wall and is a function of the Reynolds

number and the hydraulic roughness of the wall. For example, for pipe flow through hydraulically smooth tubes^{11,13}

$$f = 0.079 \text{Re}^{-0.25} \quad (2a)$$

$$\sim 2.3 \times 10^3 \leq \text{Re} \leq \sim 10^5$$

or

$$f = 0.046 \text{Re}^{-0.2} \quad (2b)$$

$$\text{Re} \geq \sim 10^5$$

In hydraulically rough tubes, the relationship changes,¹¹ but usually cannot be evaluated because the roughness factor is unknown.

The hypothesis is that to ensure the same fluid-alloy interaction in the laboratory and in the plant, the apparatus used to simulate the plant geometry should be operated so that the wall shear stress range is the same as that encountered in the plant geometry. This equality may be written:

$$(\tau)_{\text{laboratory}} = (\tau)_{\text{plant}} \quad (3)$$

If Equation (3) is fulfilled experimentally, then for a given system, the mechanism by which fluid velocity affects corrosion in the plant is proposed to be identical to the mechanism by which fluid velocity affects corrosion in the laboratory. The flow regimes must be the same (e.g., both laminar or both turbulent) and satisfy the no-slip condition at the wall. The actual equation that relates corrosion rate to fluid velocity could be different in each geometry because the mathematical relationship between corrosion rate and hydrodynamics is geometry dependent.

Fulfillment of Equation (3) is the proposed method of designing a laboratory velocity test. If a velocity sensitivity is found in the laboratory, the appropriate corrosion rate-fluid mechanics relationship for the plant geometry and for the same mechanism is used to determine the expected corrosion rate in the plant. Equation (3) is general. It can be used for any plant geometry as long as the wall shear stress in the plant geometry can be estimated. The shear stress at the wall can be estimated for many geometries.¹³ No conclusive experimental proof is available for the validity of a velocity test which fulfills Equation (3). Some support for the use of Equation (3) to design a velocity test can be found in arguments discussed later.

The laboratory device used for this test is the rotating cylinder within a cylinder electrode. It was chosen because it operates in the turbulent regime over a wide range of Reynolds numbers.⁸ Many plant flows are turbulent. An example of the method used for designing a laboratory velocity test using the rotating cylinder electrode to duplicate the velocity sensitive corrosion mechanism in the plant is as follows. The plant geometry to be modeled is assumed to be pipe flow in the turbulent regime ($\text{Re} > 2300$ or so) with a wall shear stress of $(\tau)_{\text{pipe}}$.

The shear stress on the rotating cylinder is given by¹⁴

$$(\tau)_{\text{cylinder}} = \frac{f}{2} \rho \omega^2 r^2 \quad (4)$$

For a hydraulically smooth cylinder, the friction factor has been found¹⁴ to be related to the Reynolds number based on cylinder diameter by

$$\frac{f}{2} = 0.079 \text{Re}^{-0.30} \quad (5)$$

Therefore, the shear stress equation for the "hydraulically smooth" cylinder can be written as

⁽¹⁾Symbol definitions are listed in the Appendix on page 226.

$$(\tau)_{\text{cylinder}} = 0.079 \text{ Re}^{-0.30} \rho \omega^2 r^2 \quad (6)$$

The appropriate range of rotation rates can then be found by combining Equations (3) and (6) and by solving for the rotation rate $\omega = (2\pi/60 \times \text{rpm})$. Since the theory is approximate, an order-of-magnitude span of rotation rates which includes those calculated should be examined.

Experimental Apparatus

Rotating Cylinder Electrode

The laboratory apparatus is shown in Figure 1. The outer cylinder is formed by the Pyrex wall of the cylindrical vessel. A platinum screen counter electrode 7.5 cm high by 7.5 cm in diameter rests against the inside wall of the vessel. A piece of solid Teflon fits snugly into the top of the vessel. This Teflon has holes drilled in it for the Luggin-Haber capillary, a gas dispersion tube, a platinum connection to the counter electrode, and the inner rotating cylindrical working electrode. Heat can be supplied by wrapping heating tape around the outside of the vessel. The temperature is controlled by an automatic temperature controller (Model 51, Love Control Corp.).

The working electrode is shown in Figure 2. The electrode is composed of an inner Hastelloy G shaft which is connected to the rotator. Around its lower portion is a tightly fitting, hollow Teflon rod. This Teflon insulates the inner shaft from the outer components. The working electrode is composed of four parts. The surface to which electrical contact is made is a hollow cylinder of Hastelloy G. Resting against this cylinder is a hollow cylinder of Rulon, a hard Teflon-like material. Next is the cylindrical test coupon. Its working surface is about 2.5 cm in length. It has an unexposed surface that extends under the

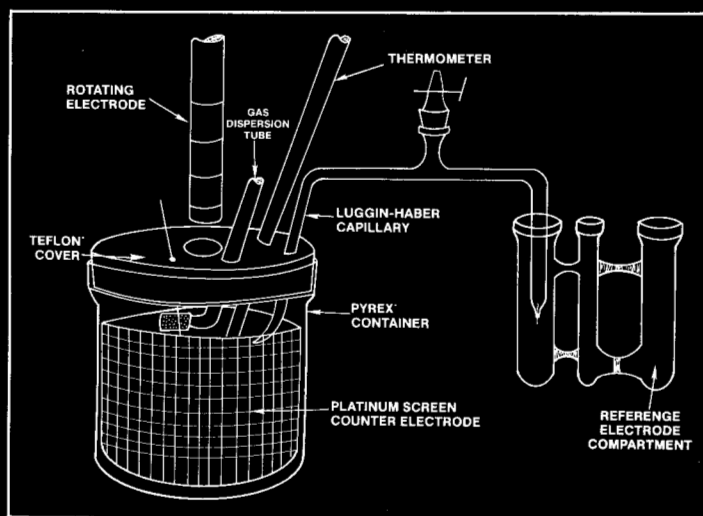


FIGURE 1 — Rotating cylinder electrode apparatus.

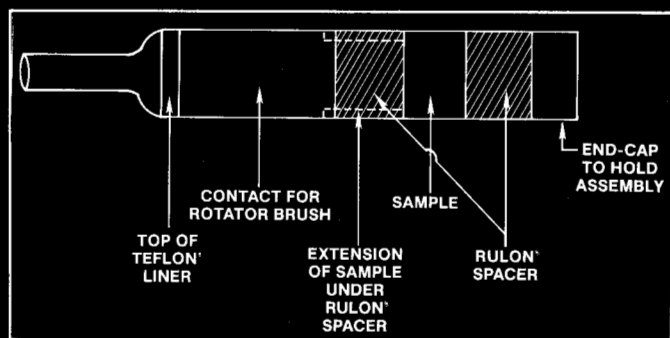


FIGURE 2 — Inner rotating cylinder used in laboratory apparatus of Figure 1.

Rulon to make electrical contact with the underside of the hollow Hastelloy G cylinder. Next is a hollow cylindrical Rulon spacer. Both spacers are used to eliminate hydrodynamic end effects. Last is a Hastelloy G bolt that attaches to the inner shaft, is electrically isolated from the working electrode, and holds the assembly together. When operating, the liquid interface is no higher than about the midpoint of the upper Rulon spacer.

The working electrode shaft is attached to an ASR2 Analytical Rotator which can rotate from 50 to 2000 rpm in the low range and 220 to 10,000 rpm in the high range. A Strobotec 1532-A strobe light has been used to check the speed control calibration.

A PAR 173D potentiostat with a 376 logarithmic convertor is used to control the potential of the test electrode relative to a remote reference electrode. A PAR 175 Universal Programmer is used to scan voltages, and a Hewlett-Packard 7045B X-Y recorder is used to record the voltage-log current curves. At present, no attempt is made to correct for the uncompensated voltage drop caused by solution resistance.

Characterization by Oxygen Reduction

Experiments were run to confirm that the rotating cylinder electrode obeys the hydrodynamics expected for this system.¹⁴ This agreement was confirmed by comparing the measured and calculated Sherwood number-Reynolds number relationship for oxygen reduction. The reduction of oxygen on Monel 400 (60-Ni, 40-Cu) in both 3 Wt% NaCl and 5 Wt% Na₂SO₄ was examined. The alloy sample was finished with progressively finer silicon carbide paper until a 400 grit finish was achieved. Two sets of experiments were run at 25 C. In the first set, the oxygen mass transfer controlled regime was confirmed to be present at -1.0 V(SCE) by measuring current vs voltage in 0.1 V increments as a function of rotation rate. Then, the sample was rotated between 100 (Re = 2000) and 6000 rpm (Re = 120,000) while controlling the voltage at -1.0 V(SCE). The current was recorded after steady state was achieved.

The calculated Sherwood numbers were plotted as log Sh/Sc^{0.356} vs log Re. All points were found to lie within about 10% (1 standard deviation) of the Eisenberg, *et al.*, curve.¹⁴ This agreement means that Equation (6) can be used to calculate the friction factor for a hydraulically smooth cylinder.

Example of Application of Rotating Cylinder Electrode

Introduction

Flowing acetone cyanohydrin has been found to cause corrosion of mild steel. This corrosion has tended to be a combination of localized areas of attack with elongation in the flow direction as well as thinning of the wall. The question arose as to whether this attack is strongly dependent on fluid flow. The thinning and oblong nature of the localized areas suggested that the corrosion mechanism has a fluid velocity sensitivity. The rotating cylinder electrode was used to determine if such a sensitivity exists.

Experimental Design

The appropriate rotation rates were determined from the data shown in Table 1. Equations (1) and (2a) were used to calculate the wall shear stress in the pipe. The rotation rate that yields a comparable shear stress was calculated by inserting Equation (6) into Equation (3) and by solving for the rotation rate. The rotation rate obtained is about 3500 rpm. Since this approach is still tentative, rotation rates of 500 and 5000 rpm were used in the laboratory simulation.

Two types of experiments were run—polarization scans and long-term (24 h) corrosion rate determinations. No attempt was made to correct for the voltage drop caused by uncompensated solution resistance (conductivity ~ 100 $\mu\text{mho cm}^{-1}$) and for junction potentials. This procedure precludes the corrosion

TABLE 1 — Pipe Flow Data

Property	Value
Flow velocity	$5.40 \times 10^2 \text{ cm s}^{-1}$
Pipe diameter	$1.02 \times 10 \text{ cm}$
Viscosity	$9 \times 10^{-2} \text{ g cm}^{-1} \text{ s}^{-1}$
Density	$9.3 \times 10^{-1} \text{ g cm}^{-3}$
Reynolds number	5.68×10^4

TABLE 2 — Time to Reach Steady-State Corrosion Potential

Rotation Rate (rpm)	Time (min)
0	4.3
500	1.9
5000	8.5×10^{-1}

rate from being determined by monitoring a current at a controlled voltage.¹ However, the corrosion rate could still be determined from the weight loss after 24 h. The acetone cyanohydrin was at about 99% purity, a small amount of sulfuric acid being present in the hydrocarbon.

The procedure was to obtain the steady-state corrosion potential and begin the scan at this potential. All scan rates were run at 1.8 V/h (0.5 mV/s). A saturated calomel electrode (SCE) was used, and all reported voltages are relative to this reference. All experiments were at room temperature. The mild steel samples were sanded with progressively finer silicon carbide paper until 600 grit was used. The impurity content of the steel was within the ASTM specification A 106.

Long-term 24 h experiments were run at constant rotation rates of 500 and 5000 rpm. The corrosion potential was monitored. Polarization scans were run in the solution at the conclusion of each experiment. The surface of the mild steel was again progressively finished so that the last sanding was with 600 grit silicon carbide paper. Weight loss was measured. Solution samples were taken after 30 min, 60 min, 4 h, and 24 h of rotation for ICAP (Inductively coupled argon plasma) analysis. The purpose was to estimate the degree of mass transfer control by assuming that dissolution of Fe^{+2} is the rate determining step.

Results

The corrosion potential was monitored until approximate steady state was reached. Steady state was reached in the 24 h runs discussed later. In all cases, the corrosion potential started at about 0.55 V and then quickly dropped to about -0.13 V. The value of the final corrosion potential is virtually independent of velocity. However, the time to reach within 5 to 10 mV of that potential is dependent on velocity as shown in Table 2. This velocity dependence on the time to reach steady state suggests that the rate of breakdown of any passive film on the steel has a velocity sensitivity.

Figures 3, 4, and 5 show polarization scans under stagnant conditions and at 500 and 5000 rpm. Forward polarization was stopped after the current dropped to a low value, suggesting some type of passivation. Since the voltage drop between the Luggin-Haber capillary and the electrode surface remained uncompensated, absolute values of current and voltage are semiquantitative at best. However, differences in these values are still significant.

Two other polarization scans were run in which the polarization was stopped prior to passivation at the rotation rate used. In the first case, the voltage was held at a potential

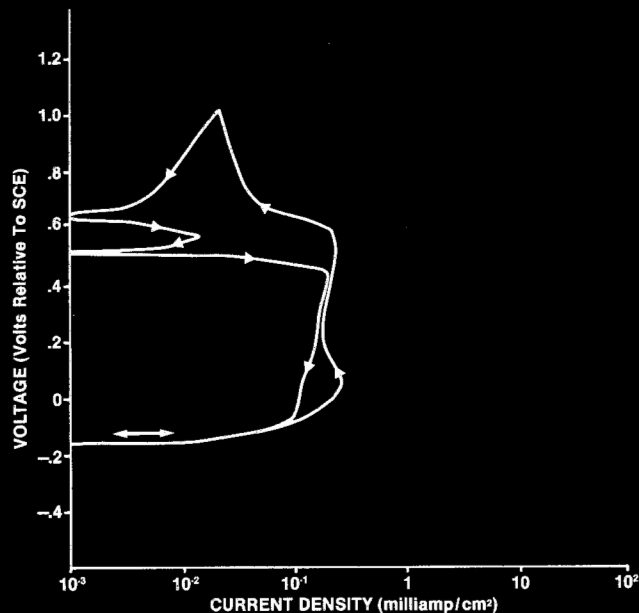


FIGURE 3 — Polarization scan of carbon steel in acetone cyanohydrin, 1.8 V/h, 25 C, 0 rpm.

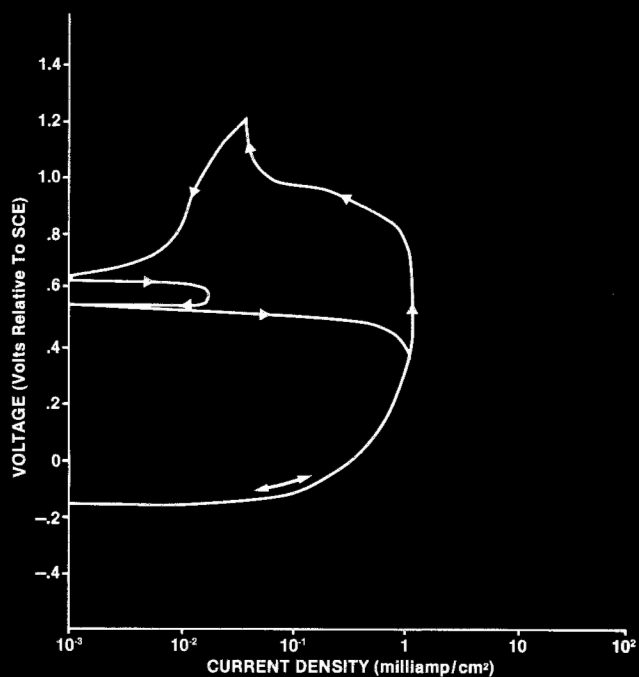


FIGURE 4 — Polarization scan of carbon steel in acetone cyanohydrin, 1.8 V/h, 25 C, 500 rpm.

anodic to the potential corresponding to passivation at 0 rpm while the rotation was stopped for a period of time. Then the rotation was resumed, and the scan was reversed. In the second case, the scan was immediately reversed at constant rotation. Examples of the first and second scans are shown in Figures 6 and 7, respectively. Both are at 500 rpm. Results at 5000 rpm were similar (not shown).

The weight loss results for the 24 h experiments are shown in Table 3. Problems arose with some of the ICAP analyses, most likely during "digestion" of the acetone cyanohydrin during preparation. For example, one sample was lost because of bubbling.

Discussion of Experimental Results

Polarization Scans. Figure 3 shows a polarization scan in stagnant solution. Once the voltage passes 0.55 to 0.60 V, carbon

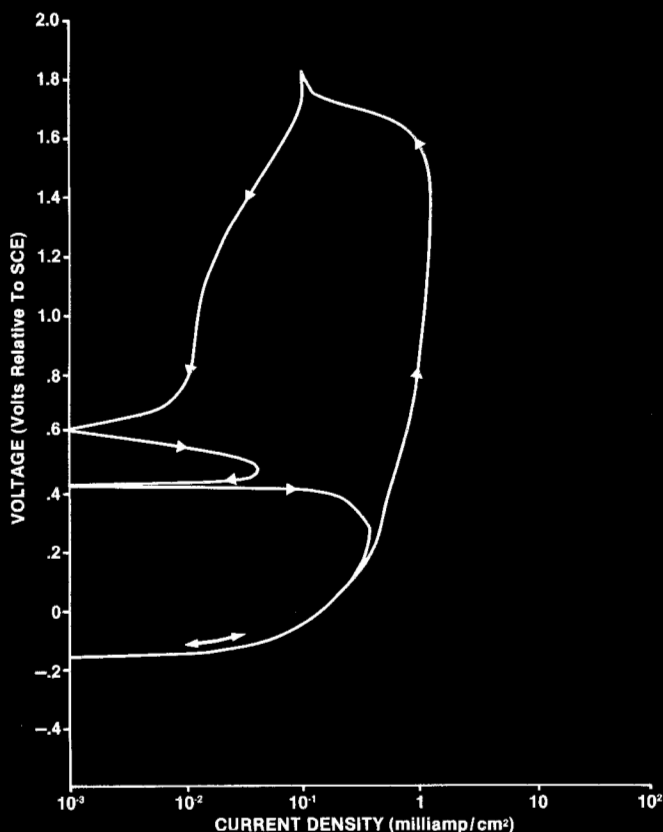


FIGURE 5 — Polarization scan of carbon steel in acetone cyanohydrin, 1.8 V/h, 25 C, 5000 rpm.

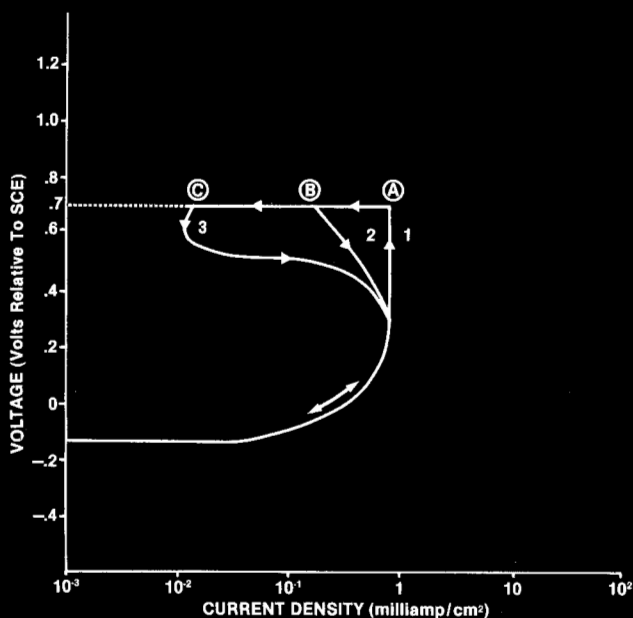


FIGURE 6 — Polarization scans of carbon steel in acetone cyanohydrin, 1.8 V/h, 25 C, 500 rpm. Curve 1, forward scan. Curve 2, reverse scan after 10 min pause at 0 rpm. Curve 3, reverse scan after 35 min pause at 0 rpm.

steel attempts to passivate. Possibly, this transition corresponds to the formation of a solid surface film containing Fe(III). Upon decreasing the potential, the film would be reduced to Fe(II) (first peak), and after reduction, the curve is suggestive of active corrosion.

The important attribute is the ease with which the oxidized surface film seems to be reduced. Iron (III) is probably not present at the steady-state corrosion potential. To determine if this 0.55 V is critical, another polarization scan was run

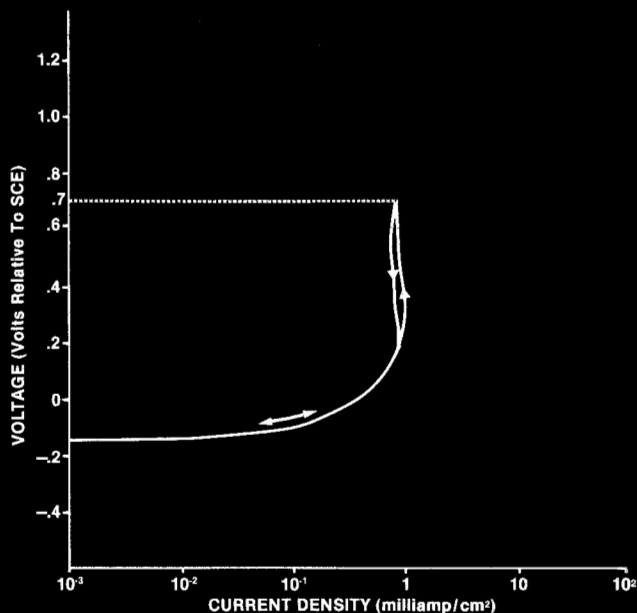


FIGURE 7 — Polarization scan of carbon steel in acetone cyanohydrin, 1.8 V/h, 25 C, 500 rpm. Scan reversed immediately after 0.7 V was reached.

TABLE 3 — Weight Loss and Characteristics of Long-Term Experiments

Rotation Rate (rpm)	Comments
0	Stagnant conditions for 66 h; total weight loss = 0.0055 g; weight loss/24 h = 0.002 g
500	Continuous for 24 h; weight loss = 0.0119 g
5000	Continuous for 24 h; weight loss = 0.0267 g (Repeat experiment, weight loss = 0.0256 g)

to 0.50 V and held for 45 min (not shown). The return scan virtually retraced the forward scan. This 0.55 V must be exceeded for passivation to occur; a critical passivation voltage exists. Note that 0.55 V corresponds to the potential measured immediately after immersion of the samples.

These phenomena were studied as a function of velocity. A polarization scan was repeated at 500 rpm. This scan, shown in Figure 4, shows one important difference from that in Figure 3. The onset of passivation in the forward (positive) scan occurs at 0.80 V. The point where passivation begins in the forward scan is a function of velocity. The return (negative) scan has anodic to cathodic transitions similar to those at 0 rpm, suggestive of reduction of a surface film. In fact, this reduction again begins in the range of 0.50 to 0.60 V, the place where passivation occurs at 0 rpm.

The experiments were rerun at 5000 rpm to further examine this effect. Figure 5 shows the polarization scan. The apparent primary passivation potential is pushed to between 1.2 and 1.3 V. The interesting point is that mild steel again loses passivity in the return scan between 0.50 and 0.60 V, the place where passivity occurs at 0 rpm.

The results of an initial attempt to study the effect of velocity are shown in Figure 6. For this complex experiment, the potential was scanned (curve 1) from the corrosion potential to 0.70 V (point A). The rotator was stopped for 10 min while the voltage was maintained at 0.70 V. The current fell to point B. Rotation was resumed, and the potential scan direction was reversed. The current-voltage curve followed is curve 2. When

the corrosion potential was reached, the voltage was immediately set to 0.70 V. The current-voltage response returned to point A. Rotation was stopped for 35 min, and the current fell to point C. Rotation was resumed, and the voltage was scanned back to the corrosion potential. The response is shown on curve 3.

The importance of this experiment is as follows. The conductivity of the solution is low. At the high current densities expected for mass transfer domination of the corrosion rate (1 to 100 mA/cm²), lack of compensation of solution voltage drop can result in distortions of the polarization scan. As shown by Mansfeld,¹⁵ this distortion would make the primary passivation potential appear to move in the anodic direction. Most likely, the higher the current, the larger the distortion and the farther the primary passivation potential would appear to move. When the rotation is stopped, the current drops, the distortion decreases, and the effective voltage rises above the actual primary passivation potential. With time, the more passive film is established. Indeed, if rotation is not stopped, the effective voltage cannot become greater than the primary passivation potential, and the steel cannot passivate (Figure 7). These results suggest that the current density at the anodic nose increases with fluid velocity. Thus, the corrosion rate is highly dependent on fluid velocity.

Long-Term Experiments. An estimate of the degree of mass transfer control was made. First the mass transfer coefficient was estimated by the Eisenberg, *et al.*,¹⁴ correlation

$$Sh = 0.079 Re^{0.7} Sc^{0.356} \quad (7)$$

The value of the estimated mass transfer coefficient, $k (= Sh D/d)$ was compared to that estimated from the 24 h weight loss data. A time-averaged Sherwood number was calculated by

$$\bar{Sh} = \left(\frac{\Delta w}{Mt} \right) \left(\frac{1}{A} \right) \left(\frac{1}{C_w - C_B} \right) \frac{d}{D} \quad (8)$$

The concentration at the wall was assumed to be equal to the saturation concentration of iron. Problems with ICAP analysis precluded a measurement of this quantity. The saturation concentration was estimated by curve-fitting the iron concentrations found during the continuous 5000 rpm experiment and by extrapolating to infinite time. The estimated saturation concentration is 9.8×10^{-7} mol cm⁻³. This value was used for calculations at both 500 and 5000 rpm. This estimate must be viewed as approximate.

The physical properties used are shown in Table 4. The diffusivity of iron was assumed to be that of FeSO₄ in 68% sulfuric acid in lieu of other data.¹ The compound FeSO₄ was used to model the iron species in solution because of the sulfuric acid impurity that was present. An iron cyanide ion might have been an alternative model. Since the actual value of the diffusion coefficient may be between 10^{-7} and 5×10^{-6} cm²s⁻¹, the value shown is probably within a factor of two to four of the real value. Inserting these values into Equations (7) and (8) results in the mass transfer coefficients shown in Table 5. The predictions made by using the Eisenberg, *et al.*, correlation are included.

TABLE 4 — Physical Properties of Parameters

Property (symbol, units)	Value
Density (ρ , g cm ⁻³)	9.3×10^{-1}
Viscosity (μ , g cm ⁻¹ s ⁻¹)	9×10^{-2}
Diffusivity (D, cm ² s ⁻¹)	6×10^{-7}
Area (cm ²)	1.2×10
C _w (mol cm ⁻³)	9.8×10^{-7}

TABLE 5 — Estimated Mass Transfer Coefficients

Rotation Rate (rpm)	Method of Estimation	Mass Transfer Coefficient (cm s ⁻¹)
500	Equation (7)	2.2×10^{-4}
	Equation (8)	3.0×10^{-4}
5000	Equation (7)	1.1×10^{-3}
	Equation (8)	1.3×10^{-3}

The agreement in Table 5 indicates that mass transfer completely controls the corrosion rate, at least during the short exposures (24 h) examined. Such control usually results in general corrosion. One way to estimate the corrosion rate in pipes for this mechanism is to use the mass transfer coefficient derived for pipe flow and the relationship between mass transfer and concentration difference. The mass transfer coefficient in pipes can be estimated by the Harriott and Hamilton correlation¹⁶

$$Sh = 0.0096 Re^{0.913} Sc^{0.346} \quad (9)$$

and the mass transfer rate per unit area by

$$R = (Sh) (C_w - C_B) \frac{D}{d} \quad (10)$$

Assuming a 10.2 cm pipe diameter and a bulk iron concentration of 3.3×10^{-8} mol cm⁻³ (2 ppm), some estimated corrosion rates are shown in Table 6. These corrosion rates are dependent on the assumptions of the 9.8×10^{-7} mol cm⁻³ (59 ppm) saturation concentration, the value of the diffusion coefficient, and the possibility that the mechanism is one in which the corrosion rate is at all times *completely* controlled by the rate of mass transfer from a film saturated in an iron salt.

Unfortunately, no pipe or spool piece corrosion rates are available. The corrosion rates in Table 6 may be higher than those found in the plant because the results assume only convective mass transfer control. With exposure, a surface film often develops, or the surface may undergo a slow structural transition. Such phenomena can depress the corrosion rate by creating a second diffusional barrier to mass transfer.² Only long exposure results can uncover this behavior. In addition, there are inaccuracies in the physical constants. The important point is that the corrosion rate is very sensitive to fluid velocity, and the corrosion mechanism probably involves a high degree of iron ion mass transfer control. In a practical sense, the greater the flow rate, the greater the corrosion rate. These observations agree with the observations of the attack on the piping described earlier. The mechanism also agrees with the polarization scans suggesting velocity sensitive corrosion in the region of the corrosion potential and a velocity independent repassivation potential.

TABLE 6 — Expected Pipe Corrosion Rates Rates Under Mass Transfer Control⁽¹⁾

Fluid Velocity		Corrosion Rate	
cm s ⁻¹	ft s ⁻¹	mm y ⁻¹	(mil/y)
30.5	1	1.1×10^{-1}	4.5×10^{-1}
152.0	5	5.3×10^{-1}	2.1
305.0	10	9.9×10^{-1}	3.9
610.0	20	1.8	7.3

⁽¹⁾ Assuming 10.2 cm pipe and C_w = 59 ppm.

Discussion of Laboratory Simulation Theory

The use of Equation (3) to develop a velocity sensitivity test lacks conclusive experimental verification. At this point, it is only hypothesis. Some support for Equation (3) can be found for the cases of complete or even partial mass transfer control of corrosion. The friction factor may often be related to the Sherwood number through the Chilton-Colburn analogy.¹²⁻¹⁴

$$\frac{Sh}{Re \times Sc} = \frac{f}{2} \phi(Sc) \quad (11)$$

This equation has been verified for a number of geometries. In Equation (11), the empirical factor f that quantifies the friction or momentum transfer (velocity profile) which gives rise to shear stress may be related directly to the Sherwood number which contains the mass transfer coefficient. Hence, mass transfer has a relationship to shear stress. This relationship depends on the ratio of the hydrodynamic boundary layer thickness to the mass transfer boundary layer thickness. This ratio of boundary layer thicknesses is a function of the Schmidt number raised to an exponent.¹³ In many geometries, this exponent lies between 0.3 and 0.4.^{1,12-14} If the alloy and fluid are the same in different geometries, the relationship between the ratios of the boundary layer thicknesses in the geometries becomes a function of the Schmidt number raised to only a small exponent. Thus, for a given fluid-alloy system, the thickness ratio of these boundary layers seems to have only a slight dependence on geometry. In addition, if the flow regimes in the two geometries are the same, laminar or turbulent, and there is no slip at the wall, then the parameters describing the momentum transfer have a similarity in different geometries.¹⁷ This similarity suggests that equating of shear stresses may be a reasonable method of enabling the momentum transfer mechanisms to have a similarity in the two geometries. Thus, by the analogy of Equation (11), the similarity in momentum transfer suggests a comparable similarity in the mass transfer mechanism for a given fluid-alloy system in different geometries.

Support for these arguments can be found in this study in which by matching in the laboratory the range of shear stresses found in plant piping, a mass transfer controlled corrosion rate was detected experimentally. Velocity sensitive corrosion had been observed in the plant. Support can also be found in the work of Ellison and Schmeal, who showed that a mass transfer controlled model for carbon steel corrosion in sulfuric acid explains the data for both pipe and rotating cylinder geometries.¹ The range of shear stresses used in the pipe geometry overlapped the range of shear stresses used in the rotating cylinder geometry. Thus, Equation (3) was fulfilled to some degree during these experiments in which complete mass transfer control was found in different geometries.

In addition, fluid velocity can affect the corrosion rate through erosion. Efird³ has shown that once the flow of seawater through copper-nickel alloys becomes greater than a certain shear stress in pipe flow, erosion accelerates the corrosion rate. Shear stress seems to be the governing variable. This point led Efird to conclude that the concept of critical shear stress could be applicable to other geometries handling seawater. If both geometries operate in the same turbulent or laminar flow regimes, the above arguments suggest that the breakaway shear stresses in both geometries could be comparable for the same alloy. Indeed, if erosion in other alloy-environment systems depends only on shear stress, then fulfilling Equation (3) while maintaining the same flow regime may allow one geometry to model erosion-corrosion mechanistically for another geometry. Such mechanistic modeling would not necessarily mean that the corrosion rates are the same in the two geometries at the same shear stress.

One final point should be mentioned. When the corrosion process creates a rough surface, the corroding cylinder would most likely be rough. The friction factor and subsequent velocity sensitivity would be a function of this roughness.¹⁶

Also, if the film creates an added impediment to mass transfer, a dampening of the velocity dependence may occur.² Quantitative knowledge of either the roughness factor or the dampening is usually not available. Under these conditions, Equation (3) would be used to construct the test, assuming a smooth wall [e.g., Equation (6)]. Deviations could then be examined in terms of how these types of extraneous effects might affect the shear stress and corrosion mechanism.

Acknowledgment

The author would like to thank M. E. Zerr of the Materials Laboratory at Monsanto for her active participation in the design and running of the acetone cyanohydrin experiments. The author also thanks P. Medina for performing the oxygen reduction experiments.

References

1. B. T. Ellison and W. R. Schmeal, *J. Electrochem. Soc.*, Vol. 125, p. 524 (1978).
2. B. K. Mahato, C. Y. Cha, and L. W. Shemilt, *Corros. Sci.*, Vol. 20, p. 421 (1980).
3. K. D. Efird, *Corrosion*, Vol. 33, No. 1, p. 3 (1977).
4. G. B. Hatch and O. Rice, *Ind & Eng. Chem.*, Vol. 37, p. 752 (1945).
5. NACE Standard, TM-02-70, "Method of Conducting Controlled Velocity Laboratory Corrosion Test," October, 1970.
6. F. Opekar and P. Beran, *J. Electroan. Chem.*, Vol. 69, p. 1 (1976).
7. D-T. Chin, *AIChE J.*, Vol. 20, No. 2, p. 245 (1974).
8. D. R. Gabe, *J. Appl. Electrochem.*, Vol. 4, p. 91 (1974).
9. V. M. Novakovskii and S. N. Fishman, *Trudy Ural'Skogo Nauchno-Issled Khim. Inst.*, Vol. 9, p. 71 (1962).
10. V. Yu. Filinovskii, B. L. Reizen, I. V. Strizkevskii, M. R. Tarasevich, and B. P. Pribytko, *Zashch. Met.*, Vol. 12, p. 672 (1976).
11. H. Schlichting, *Boundary Layer Theory*, McGraw-Hill Book Co., New York, 1979.
12. T. H. Chilton and A. P. Colburn, *Ind. Eng. Chem.*, Vol. 26, p. 1183 (1934).
13. W. M. Kays, *Convective Heat and Mass Transfer*, McGraw-Hill Book Co., New York, 1966.
14. M. Eisenberg, C. W. Tobias, and C. R. Wilke, *J. Electrochem. Soc.*, Vol. 101, No. 6, p. 306 (1954).
15. F. Mansfeld, *Corrosion*, Vol. 38, No. 10, p. 556 (1982).
16. P. Harriott and R. M. Hamilton, *Chem. Eng. Sci.*, Vol. 20, p. 1073 (1965).
17. T. Theodorsen and A. Regier, *NACA Report 793*, 1945.
18. R. Kappesser, I. Cornet, and R. Greif, *J. Electrochem. Soc.*, Vol. 118, No. 12, p. 1957 (1971).

Appendix—Definitions of Symbols

A	= area (cm ²)
C_B	= bulk concentration (mol cm ⁻³)
C_w	= wall concentration (mol cm ⁻³)
d	= diameter of cylinder (cm)
D	= diffusion coefficient (cm ² s ⁻¹)
f	= friction factor (dimensionless)
F	= Faraday's constant (coul equiv ⁻¹)
k	= mass transfer coefficient (cm s ⁻¹)
M	= molecular weight (g mol ⁻¹)
n	= equivalent mole ⁻¹
r	= radius of cylinder (cm)
R	= corrosion rate (mol cm ⁻² s ⁻¹)
Re	= Reynolds number ($\rho u d / \mu$)
Sc	= Schmidt number (ν / D)
Sh	= Sherwood number ($k d / D$)
t	= time (s)
u	= velocity (cm s ⁻¹)
w	= weight (g)
μ	= absolute viscosity (g cm ⁻¹ s ⁻¹)
ν	= kinematic viscosity (μ / ρ) (cm ² s ⁻¹)
ρ	= density (g cm ⁻³)
τ	= wall shear stress (g cm ⁻¹ s ⁻²)
ω	= rotation rate (radians s ⁻¹ = (2 π)RPM/60)